Dynamic Modeling of a Basilisk Lizard Inspired Quadruped Robot Running on Water

Hyun Soo Park, Steven Floyd, and Metin Sitti
NanoRobotics Laboratory, Department of Mechanical Engineering,
Carnegie Mellon University, Pittsburgh, PA 15213

***Abstract*— This paper proposes a 3-D dynamic simulation of a previously developed basilisk lizard inspired quadruped robot, which is capable of locomotion on the surface of water. Using this 3-D simulation along with several 1-D and 2-D models, stability in terms of robot elevation from the water surface and robot rolling are examined. Analysis of the lifting force shows the robot is capable of running on water using viscous drag forces. Using this analysis, a criterion for convergence to a steady state distance from the water is presented. It is determined that 7-12 Hz is an appropriate running frequency range for the robot to lift its weight. Compliant footpads are found to be beneficial in reducing the force associated with pulling out of the water. Further, from the roll motion analysis, previous designs result in instability along the roll axis. By comparing leg running frequency to the body's roll frequency, the minimum required roll moment of inertia for stable roll motion can be determined.**

I. Introduction

Small animals and insects utilize diverse techniques to float and locomote upon the water's surface. For example, water striders and spiders, which are very light-weight insects, use surface tension [1], [2]. Heavier animals, such as basilisk lizards, dominantly use the drag forces exerted by the fast motion of their feet on the water, and take advantage of hydrodynamics for locomotion [3], [4]. A basilisk lizard's ability to locomote on both land and water using the same legged running mechanism would be a desirable trait for mimicry in robots. Such an ability will extend insight into both nature and potential robotics applications.

Biomimetic robots are machines which emulate some aspect of a living system. This work describes the dynamics of a biomimetic robot which runs on the surface of water in a manner similar to the basilisk lizard. Unlike other aquatic and amphibious robots which swim or walk through the water [5], [6], [7], [8], the water runner can stride upon it. This robot employs momentum transfer for both lift and propulsion, with negligible use of surface tension or buoyancy, which other water walking robots employ [9], [10], [11]. Hence, the robot is the lightest of the amphibious robots, but the heaviest of the robots which locomote by water walking.

Computer modeling enables us to understand and to analyze complex dynamics by adopting appropriate numerical integration algorithms, such as the Runge-Kutta method [12], [13]. In particular, designing and simulating complex robotic systems helps to determine their performance in dynamic environments, such as a fluid surface, and to determine optimal parameters for physical prototypes. Using an experimental model of the quadruped water running robot (Fig. 1), a 3-D dynamic simulation based on the original CAD model was developed in a virtual environment. Software *piroCORE* that includes a dynamic engine library which facilitates kinematics and dynamics has been used to simulate and animate the virtual robot. This paper models how a water running robot similar to the basilisk lizard can traverse the water's surface and broadens our understanding of its legged dynamics.

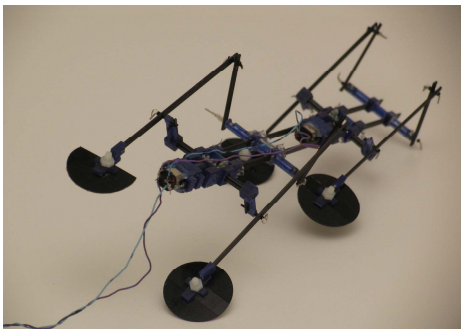

Fig. 1. Photograph of the four-legged robot inspired by basilisk lizards.

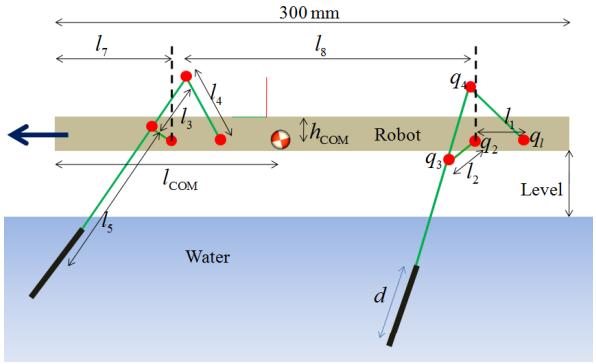

Fig. 2. Schematics of the basic geometry and dimensions of the robot. Lengths of the four bar mechanism are given in Table I.

II. Robot Model Description

The water running robot has a mass of approximately 60 g, contains two miniature DC motors, and has four legs as shown in Fig. 1. It is 300 mm long, 60 mm wide, and most of its mass is concentrated at the center where the

Robot Specification		Link Length	
Robot Length (cm)	30	l_1 (cm)	6.15
Robot Width (cm)	6.32	l_2 (cm)	2.18
Robot Mass (kg)	0.06163	l_3 (cm)	7.48
Moment of Inertia		l_4 (cm)	4.68
Roll (kg m^2)	3.99×10^{-5}	l_5 (cm)	6.24
Pitch (kg m^2)	5.31×10^{-4}	l_6 (cm)	5.375
Yaw (kg m^2)	5.32×10^{-4}	l_7 (cm)	17.325
Center of Mass (COM) and Footpad			
l_{COM} (cm)	12.9		
h_{COM} (cm)	1.1		
d (cm)	4		

TABLE I
ROBOT SPECIFICATIONS AND DIMENSIONS.

motors are located. Geometric relations are labeled in Fig. 2 and referenced in Table I. It uses two double-sided four-bar mechanisms which are cyclically actuated, one in the front and one in the rear, in order to run on the water. Each foot can be either a 40 mm rigid circle, or a circular foot with compliant flaps that fold to reduce undesired drag. Further information on the behavior of the water runner robot can be found in [4].

Two velocity controllers are used to actuate the simulated robot, one for each motor. These controllers compute the errors of acceleration, velocity, and position, and apply the critical gain necessary to make the error in velocity converge to zero as quickly as possible. Furthermore, the inverse dynamics are used to preshape the control inputs, and applied to the model in addition to the proportional feedback control so that the velocity controllers achieve the desired velocity profile.

III. ROBOT KINEMATICS AND DYNAMICS

A. Recursive Body Kinematic Formulation

Body kinematics are formulated using the forward kinematics of open chains, which describe body twist in terms of the base body twist, V_1, and the joint angle velocity of the generalized coordinate, $\dot{q}$. Thus, the body twist of all links in each four bar linkage can be derived as follows:

$$V_i = L_i V_1 + J_i \dot{q} \tag{1}$$
$$\dot{V}_i = \dot{L}_i V_1 + L_i \dot{V}_1 + \dot{J}_i \dot{q} + J_i \ddot{q} \tag{2}$$

where L_i is the body Jacobian matrix which transforms the base body twist, V_1, from the base frame $\{1\}$ to the body frame $\{i\}$ and J_i is the joint Jacobian matrix which maps the joint angular velocity to the relative body twist with respect to the frame $\{i\}$ [14], [15]. Thus, the body twist V of each link can be derived as follows:

$$\begin{aligned}
V_{l_2} &= ({}^{1}\mathrm{Ad}_{l_2}^{-1})V_1 + E_2\dot{q}_2 \\
V_{l_3} &= ({}^{l_2}\mathrm{Ad}_{l_3}^{-1})({}^{1}\mathrm{Ad}_{l_2}^{-1})V_1 + ({}^{l_2}\mathrm{Ad}_{l_3}^{-1})E_2\dot{q}_2 + E_3\dot{q}_3 \\
V_{l_4} &= ({}^{l_3}\mathrm{Ad}_{l_4}^{-1})({}^{l_2}\mathrm{Ad}_{l_3}^{-1})({}^{1}\mathrm{Ad}_{l_2}^{-1})V_1 \\
&\quad + ({}^{l_3}\mathrm{Ad}_{l_4}^{-1})({}^{l_2}\mathrm{Ad}_{l_3}^{-1})E_2\dot{q}_2 + ({}^{l_3}\mathrm{Ad}_{l_4}^{-1})E_3\dot{q}_3 + E_4\dot{q}_4
\end{aligned} \tag{3}$$

where E_i is the joint Jacobian vector for each joint which maps the joint space to the task space. Since all joints are revolute, $E_i = \begin{bmatrix}0 & 0 & 0 & 0 & 0 & 1\end{bmatrix}^T$. The body Jacobian matrix and the joint Jacobian matrix can then be set to:

$$\begin{aligned}
L_{l_1} &= {}^{1}\mathrm{Ad}_{l_2}^{-1} \\
J_{l_1} &= \begin{bmatrix}E_2 \mid 0 \mid 0\end{bmatrix} \\
L_{l_2} &= ({}^{l_2}\mathrm{Ad}_{l_3}^{-1})({}^{1}\mathrm{Ad}_{l_2}^{-1}) \\
J_{l_2} &= \begin{bmatrix}({}^{l_2}\mathrm{Ad}_{l_3}^{-1})E_2 \mid E_3 \mid 0\end{bmatrix} \\
L_{l_3} &= ({}^{l_3}\mathrm{Ad}_{l_4}^{-1})({}^{l_2}\mathrm{Ad}_{l_3}^{-1})({}^{1}\mathrm{Ad}_{l_2}^{-1}) \\
J_{l_3} &= \begin{bmatrix}({}^{l_3}\mathrm{Ad}_{l_4}^{-1})({}^{l_2}\mathrm{Ad}_{l_3}^{-1})E_2 \mid ({}^{l_3}\mathrm{Ad}_{l_2}^{-1})E_3 \mid E_4\end{bmatrix}.
\end{aligned} \tag{4}$$

B. Accumulated Multibody System Method: Principle of Dynamical Balance

Dynamics of the robot are derived from the principle of dynamical balance, which utilizes the Newton-Euler equation for single body motion and yields an equation of motion for the composite system by using D'Alembertian wrench [15]. This method encapsulates the internal reaction wrench of a single body and provides a generalization for obtaining the system equation of motion, which has a closed-form, instead of using the Lagrangian equation of motion. The equation of motion of the robot can be described by:

$$WF + L\tau = M\begin{bmatrix}\dot{V}_1 \\ \ddot{q}\end{bmatrix} + C\begin{bmatrix}V_1 \\ \dot{q}\end{bmatrix} \tag{5}$$

where the system wrench, $F = \begin{bmatrix}{F_{l_1}}^T \mid {F_{l_2}}^T \mid {F_{l_3}}^T \mid {F_{l_4}}^T\end{bmatrix} \in \mathbb{R}^{6\times 4}$, and the the system torque, $\tau = \begin{bmatrix}\tau_2 & \tau_3 & \tau_4\end{bmatrix} \in \mathbb{R}^3$. Gravitational forces and all the other external wrenches are lumped into F. The matrices M and C are the system inertia, including accumulated inertia by distal bodies, and the bias matrix, including centrifugal and Coriolis effects, respectively. The system torque and wrench influence matrices can be decomposed as

$$W = \left[\begin{array}{c|c|c|c} I_6 & {}^{1}\mathrm{Ad}_{l_2}^{-T} & {}^{1}\mathrm{Ad}_{l_3}^{-T} & {}^{1}\mathrm{Ad}_{l_4}^{-T} \\ 0_{6\times 6} & \widetilde{E_2^T} & \widetilde{E_2^T}({}^{l_2}\mathrm{Ad}_{l_3}^{-T}) & \widetilde{E_2^T}({}^{l_2}\mathrm{Ad}_{l_4}^{-T}) \\ 0_{6\times 6} & 0_{6\times 6} & \widetilde{E_3^T} & \widetilde{E_3^T}({}^{l_3}\mathrm{Ad}_{l_4}^{-T}) \\ 0_{6\times 6} & 0_{6\times 6} & 0_{6\times 6} & \widetilde{E_4^T} \end{array}\right]$$
$$L = \begin{bmatrix}0_{6\times 3} \\ I_3\end{bmatrix} \tag{6}$$

where $\widetilde{E_i^T} = E_i^T({}^{l_i Jl_{(i-1)}}\mathrm{Ad}_{l_i}^{-T})$. The frame $\{l_i Jl_{(i-1)}\}$ is the joint frame connecting body i with body $(i-1)$ at the body i. Then, the D'Alembertian wrench can be denoted by

$$F^* = WF + L\tau - M\begin{bmatrix}\dot{V}_1 \\ \ddot{q}\end{bmatrix} - C\begin{bmatrix}V_1 \\ \dot{q}\end{bmatrix}. \tag{7}$$

The equation of motion described in (5) is not practically useful because the simulation includes a constraint which reduces the system to one degree of freedom. Using a singular value decomposition with D'Alembertian wrench, $F^* = 0$ in (7), equation (5) is reduced to

$$W_r F + L_r\begin{bmatrix}\tau \\ \tau_l\end{bmatrix} = M_r\dot{y} + C_r y \tag{8}$$

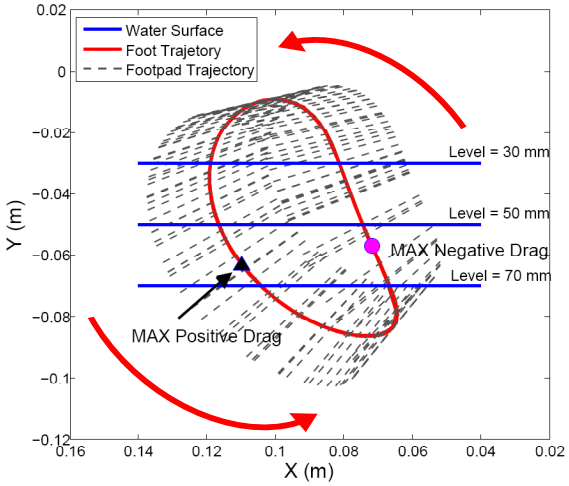

Fig. 3. Simulated trajectory of the foot with footpad orientation shown. Maximum drag occurs when the footpad plane is normal to the foot's velocity. The circle and triangle represent the position of minimum drag and maximum drag, respectively.

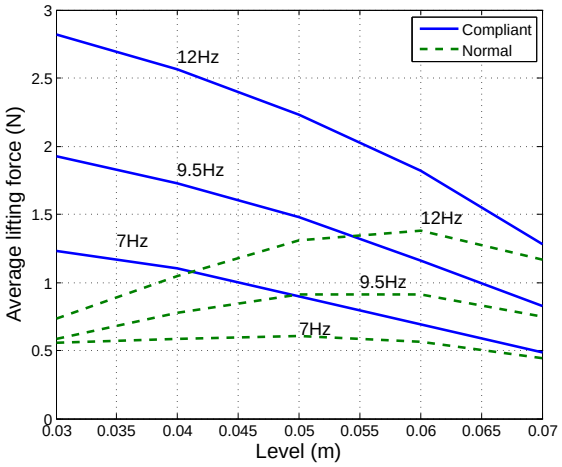

Fig. 4. Simulated overall lift force on four legs at 7-12 Hz leg rotation speed. A maximum lift occurs with a rigid foot but lift continues to increase with decreasing separation for a compliant foot.

where τ_l is the loading torque applied at a constrained joint and y represents the reduced independent joint space parameterized by the real joint space. Then, matrices W, L, M, and C are transformed to W_r, L_r, M_r, and C_r, respectively, which correspond to the independent joint space. Using (8), the equation of motion of the constrained system, the four bar mechanism, can be formulated. This kinematic and dynamic formulation is based on one leg. Since the robot has four legs with two actuators, (8) is extended to $y \in \mathbb{R}^2$.

IV. Water Interaction Modeling

A. Footpad Design

Two footpad designs are used in the simulation. One is a simple circular footpad and the other is a directionally compliant footpad which can fold. When the foot is removed from the water, the normal velocity becomes negative, which causes an undesired pulling off force. These forces are exerted over a short period of time but since this occurs during the period of maximum velocity, shown in Fig. 3, the total momentum change becomes significant. The directionally compliant footpad is introduced to reduce these effects. When pulling out of the water, two flaps on the front and the back of the foot can collapse downwards, reduced the area of the footpad normal to the velocity by 69%. This causes a significant improvement in the average lift force; an increase of about 20% in the simulation (Fig. 4). More information on the compliant footpad can be found in [16].

B. Water Interaction Integration

The forces exerted on the feet are composed of hydrostatic and hydrodynamic forces. Hydrostatic force is a buoyant force which is proportional to the depth the foot is submerged in the water. Since it is assumed that the velocity of the footpad is large enough to create an air cavity when the foot strikes the water, the hydrostatic force is equal to hydrostatic pressure multiplied by the area of the bottom of the air cavity. Most of the force is due to hydrodynamic force that acts in a direction normal to the footpad. It is proportional to the instantaneous normal velocity of the footpad and the contact area with the water. Further, it is assumed that the running frequency is low enough that the air cavity has already collapsed before the foot re-enters the water. From inspection of high speed camera footage, it is known that approximately 12 Hz is the maximum frequency at which this assumption holds.

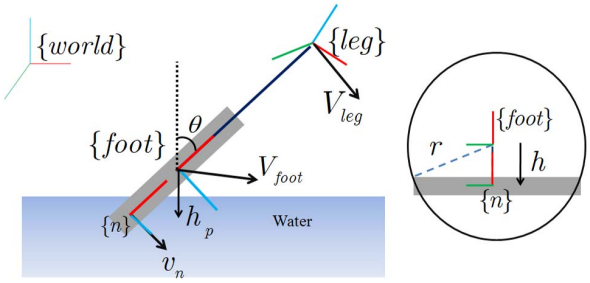

Fig. 5. Footpad geometry and the associated reference frames.

To compute the water interaction force, an integral over the submerged area is performed. Each footpad area is divided into infinitesimal area segments which contain reference frames so that one can find the velocity and position from recursive kinematic relations in (1). Body twist at the frame $\{n\}$, and the frame of an infinitesimal area are shown in Fig. 5, and can be derived from the body twist at the frame $\{leg\}$ as

$$V_n = {}^{foot}\mathrm{Ad}_n^{-1}\,{}^{leg}\mathrm{Ad}_{foot}^{-1} V_{leg}$$
$$v_n = \begin{bmatrix} 0 & 0 & 1 & 0 & 0 & 0 \end{bmatrix} V_n \,. \qquad (9)$$

Then, the water interaction force (f_z) and moment (τ_x) can

be integrated with respect to the frame $\{foot\}$ as

$$f_z = C_D^* \rho \int_0^a \sqrt{r^2-(y-r)^2}(v_n|v_n| + 2gh_p)\mathrm{d}y$$
$$= C_D^* \rho \sum_{k=0}^{k\Delta>a} \Delta\sqrt{r^2-(k\Delta-r)^2}(v_n|v_n| + 2gh_p) \quad (10)$$
$$\tau_x = C_D^* \rho \int_0^a (y-r)\sqrt{r^2-(y-r)^2}(v_n|v_n| + 2gh_p)\mathrm{d}y$$
$$= C_D^* \rho \sum_{k=0}^{k\Delta>a} \Delta(k\Delta-r)\sqrt{r^2-(k\Delta-r)^2}$$
$$(v_n|v_n| + 2gh_p) \quad (11)$$

where $C_D^* \approx 0.703$ is a constant drag coefficient [17], Δ is a discretized length which determines the precision of integration, and ρ is the density of water. The interval of integration and the absolute vertical position of an infinitesimal area can be determined by the following:

$$a = \begin{cases} h & \text{if } |h| < r \\ r & \text{if } |h| \geq r \end{cases}$$
$$h_p = (h - (k\Delta - r))\cos\theta \ . \quad (12)$$

The force and moment are transformed to an equivalent body wrench with respect to the frame $\{leg\}$ and set to external wrenches in (5).

$$F_{foot} = \begin{bmatrix} 0 & 0 & f_z & \tau_x & 0 & 0 \end{bmatrix}$$
$$F_{leg} = {}^{foot}\mathrm{Ad}_{leg}^{-T} F_{foot} \ . \quad (13)$$

Equation (13) is applied to each of the four legs whenever it is submerged. In the case of the compliant footpad, the area used in the integrand is different depending on the direction of the footpad's normal velocity. When pushing downward against the water, the footpad's normal vector and its velocity are the same direction, and integration is performed as in (10) and (11). When the footpad pulls back, the area of integration is reduced due to the directional compliance of the footpad. In which case, the $(k\Delta - r)$ part of (10) and (11) becomes $(k\Delta - r_R)$ where r_R is the reduced radius of the footpad which is taken as $1/4$th of the original radius.

Other forces such as surface tension and shear force are considered negligible. Especially when the pulling off force is applied, the contribution to drag due to surface tension has been examined and is of magnitude 10^{-2} when compared to the pulling off force caused by hydrodynamic force. Also since the Reynolds number is 7.2×10^4 at room temperature with a 7 Hz running speed, it is reasonable to neglect the shear force due to the dominance of inertial effects in the fluid.

V. Lift Force

The robot generates a drag force through its interactions with the water and utilizes this force for both propulsion and to stay above the water. Since the robot is not buoyant, it must have sufficient lift force to support its full weight while traversing on the water's surface.

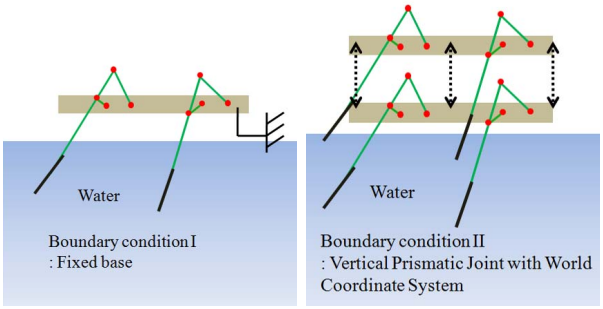

Fig. 6. Two types of boundary conditions are considered when simulating the lift force. Boundary condition I is used to measure the average lift force while varying the water level. Boundary condition II is used to determine the convergence of base body position above the water.

Modeling of the lift forces on the robot's legs is performed with two different boundary conditions. In the first, the robot is fixed at a certain height above the water. While varying both the height and the running frequency, the lift force generated by each leg and the total lift force are measured. This analysis method is useful for finding the maximum lift force at a given height above the water, to estimate how much weight the robot can sustain at that level, and to determine how robust it is when external disturbances are applied. In the second, the robot is connected to the world coordinates with a vertical prismatic joint so that it is able to move in a vertical direction. This simulation shows how the model maintains its separation from the water surface and determines whether the robot will converge to a steady state height where the overall lift force and its weight are balanced. These two boundary conditions are illustrated in Fig. 6.

A. Boundary Condition I: Fixed Base

As the robot body is placed closer to the water, lift forces become greater since the footpads remain below the water for a longer duration. During submersion, the maximum hydrodynamic force occurs soon after the whole footpad is submerged. In this region, the velocity of the footpad is nearly normal to footpad plane, as seen in Fig. 3. However, the pulling off force also becomes larger as the robot gets closer to the water and eventually surpasses the lift force, causing a net decrease in the average lift. The simulation shows that at a given running frequency, there exists a robot body separation from the water surface which yields the maximum overall lift force, as seen in Fig. 4. This is also observed in experiments, where $50 \sim 60$ mm is known to be an optimal separation. In the case of compliant feet, the pulling-out force is greatly reduced, and it never surpasses the lift force. Thus, the closer to the water the robot is located, the higher the lift force it generates.

Approximately 7 Hz is found to be the minimum frequency necessary to balance the lift force with the robot's weight, about 0.6 N, when using the rigid footpad. This result also coincides with the running frequency of real basilisk lizard on water.

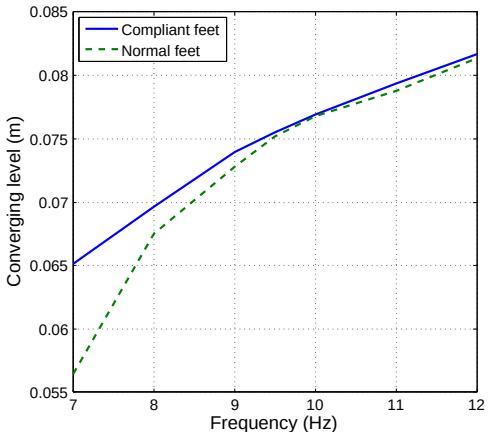

Fig. 7. Simulated steady state separation from the water as a function of running frequency for the robot iwth compliant and normal feet. Since the lift force increases with frequency, the steady state level above the water also increases.

B. Boundary Condition II: Vertical Prismatic Joint with World Coordinate System

Depending on the initial position and running frequency, the robot's vertical trajectory can be determined. If the initial position is somewhere below the elevation at which maximum lift force occurs (< 50 mm), it is unstable, especially at lower frequencies. This is because the equilibrium point where the lift force and its weight are balanced is higher than its initial location, but there is not enough lift to reach that height. Even if the running frequency is increased, and marginal stability is achieved at a level below the location of maximum lift force, any small perturbation will destabilize the robot.

For initial positions higher than the point where maximum lift force occurs, the system converges to a steady state position that is a function of running frequency, shown in Fig. 7. Higher running frequencies increase the lift force because they result in higher normal velocities and higher hydrodynamic forces inside the water. However, at very high frequencies (> 12 Hz), instantaneous forces acting on the feet are significant, and generate high instantaneous momentum in vertical direction. This in turn can cause the model to fly momentarily and splash back into the water, potentially submerging it. Once the model submerges lower than the 40 mm level, it cannot recover its position. Also, as mentioned before, high frequency running causes water interaction problems because it allows insufficient time for the air cavity to collapse. These results imply that 7-12 Hz is an appropriate frequency range to converge to a steady state position without submerging for the given robot parameters.

VI. Roll Motion Analysis

In both simulations and the experiments in [4], the robot motion in the roll direction is observed to be highly unstable because its moment of inertia is small compared to the roll moments exerted by the water contact. Thus, the above robot dynamics model is only valid when the roll motion is not considered. The key purpose of this analysis is to determine a design of the robot which is stable in the roll direction and easily controllable. Since the current model employs double sided four bar mechanisms with asymmetric leg configurations, a certain amount of roll angle variation is inevitable. The moment of inertia with respect to the roll axis of the model is 3.99×10^{-5} kg m^2 and the average moment caused by water interactions is about 3.59×10^{-2} Nm. Hence, instantaneous angular acceleration along the roll axis can exceed 900 rad/s^2 which is large enough to cause the robot to capsize.

Obviously, if the model is to locomote with a trot gait, in which diagonal pairs of feet touch the water simultaneously [18], the roll moment is always negated due to symmetry. By contrast, the worst case scenario occurs when the robot uses a pace gait, where two legs on the same side touch the water simultaneously. All other gaits will fall between these two extremes in terms of exerted roll moment. In order to create a conservative design, only the pace gait will be examined during the roll motion analysis.

Roll motion analysis is fairly complicated because it is a function of the running frequency, roll angle, instantaneous roll angular momentum, foot depth, footpad configuration and average lift force. Since several of these variables are coupled and nonlinear with respect to each other, it is impossible to do a complete analysis with this simulation alone. Hence, a simple model which is generically similar to roll motion but can be parameterized with respect to these variables is necessary. To do this, two assumptions have been made:

Assumption 1: Water interaction forces exist when the robot is tilted and are similar in magnitude and behavior to forces observed when the robot is not tilted.

Assumption 2: The water interaction force is linearly proportional to the footpad depth in the water.

Assumption 1 states that no matter what the leg configuration is, water interaction forces are always generated. Depending on the synchronization of the running frequency and the roll frequency, water interaction forces occasionally do not exist or the direction of the generated moment does not act to restore the robot. However, since increasing the running frequency can reduce this effect, and the running frequency of the current model is fairly high, Assumption 1 can be held.

Assumption 2 means that the deeper feet are, the more force is generated. This assumption comes from Fig. 4 which shows approximate linearity between the water level and the lift force. Thus, the maximum lift force is applied on a footpad when it is placed in its deepest position. As a result, it is reasonable to regard the water as a linear spring.

First, it is assumed that the robot is pivoted about a point 50 mm above the water's surface at the center of mass of the robot as in Fig. 8. This model can be parameterized as

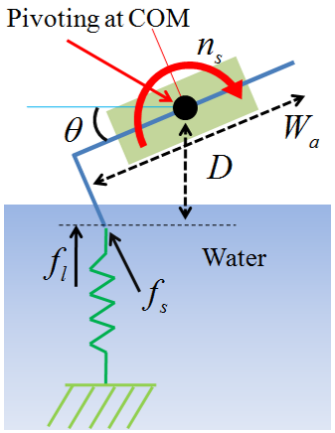

Fig. 8. Front view of the robot during roll motion modeling. The water interaction force is modeled as a linear spring with the robot pivoting about a point 50 mm above the water's surface.

follows:

$$
\begin{aligned}
D &= \frac{W_a \sin\theta}{2} + l_0 \sin\left(\frac{2\pi\theta}{4\theta_{\max}}\right)\cos\theta \\
A &= 2f_{\max}/(W_a \sin\theta_{\max} + 2l_0\cos\theta_{\max}) \\
f_l &= AD, \quad f_s = f_l \cos\theta
\end{aligned} \tag{14}
$$

where D is the linear displacement of the end of the leg, W_a is the width of the leg axis, θ is the rotation angle of the body from horizontal, $l_0 = 4.672$ cm is the maximum foot penetration depth, $\theta_{\max} = 30°$ is the desired maximum roll angle, A is the effective spring constant of the water, f_l is the lift force, f_s is the force applied to the linear spring. The maximum lift force, $f_{\max}$ at a certain frequency is chosen as $|f_{\text{lift,max}}| + |f_{\text{lift,min}}|$ since the pulling off force on one side can potentially be coupled with the maximum lift force on the other side. From f_s, the moment n_s is generated, and an ordinary differential equation can be obtained:

$$
\begin{aligned}
n_s &= -\frac{W_a f_s}{2} \\
\ddot{\theta} &= \frac{n_s}{\mathcal{I}_{roll}} \\
&= -\frac{AW_a^2 \sin 2\theta}{8\mathcal{I}_{roll}} - \frac{l_0 W_a}{2\mathcal{I}_{roll}} \sin\left(\frac{2\pi\theta}{4\theta_{\max}}\right)\cos^2\theta
\end{aligned} \tag{15}
$$

where $\mathcal{I}_{roll}$ is moment of inertia with respect to the roll axis. This modeling turns out to be remarkably similar to the actual roll motion by comparing 3D simulation.

By varying the width of the robot, the roll moment of inertia and the mass are both affected, and the modeled roll frequency, ω_{mr}, can be determined by solving (15). Conversely, (15) can also be used to determine the required moment of inertia for stability at a given running frequency.

If the roll frequency of the actual robot is greater than the running frequency, $\omega_r > \omega_{ru}$, it implies the maximum roll angle will diverge because of high angular acceleration of the body, causing the robot to capsize. If $\omega_r < \omega_{ru}$, the roll motion can be said to be stable because the lift forces on each side of the body are equal over long periods of time. But, if $\omega_r \approx \omega_{ru}$, then the robot can be marginally stable or

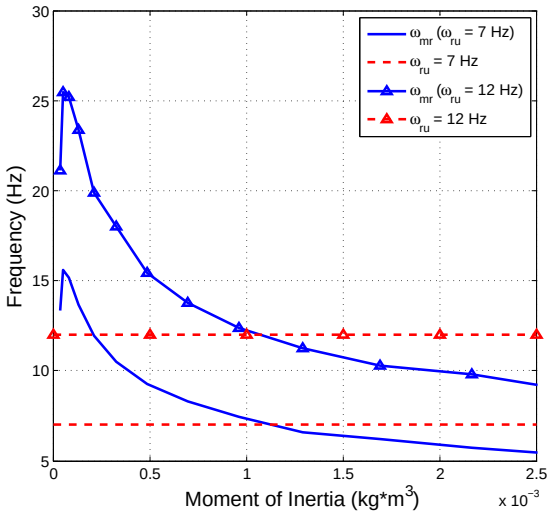

Fig. 9. Simulated relationship between the moment of inertia and the roll frequency at a running speed of 7 Hz and 12 Hz. Thus, a moment of inertia greater than approximately 1.2×10^{-3} kg m^2 is required for stability which satisfies $\omega_{mr} < \omega_{ru}$.

unstable depending on initial conditions. Since modeled roll moment is overestimation of actual roll moment for given roll moment of inertia, the fact that modeled roll motion is stable can guarantee stability of actual roll motion. Thus, one must choose a moment of inertia such that $\omega_{mr} < \omega_{ru}$ for stable roll motion (Fig. 9). Simulating with an increased roll moment of inertia, the roll angle varies less than about $\pm 6°$ and approaches steady state, which is shown in Fig. 10. The robot is oscillating less than the initially formulated $\theta_{\max} = 30°$ because (14) and (15) were formulated assuming the maximum possible lifting force, f_{max}, which may not actually occur. Therefore, using the methodology described above, a conservative estimate of the necessary roll moment of inertia for stability is produced.

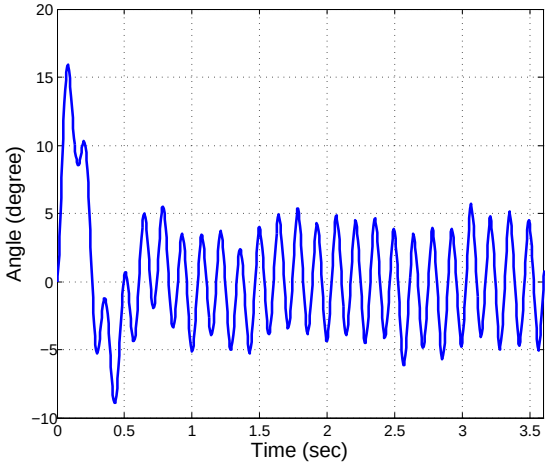

Fig. 10. Simulated variation in roll angle with an increased moment of inertia of 1.2×10^{-3} kg m^2 running at $\omega_{ru} = 7$ Hz. The roll angle varies less than about $\pm 6°$ after achieving steady state.

VII. Discussion

As a result of the roll motion analysis, it was found that roll moments of inertia greater than 1.2×10^{-3} kg m^2 lead to stable roll motion for the water runner robot parameters. The robot in [4] had a moment of inertia of only 3.99×10^{-5} kg m^2 in the roll direction, which shows that it was unstable in roll direction. To guarantee stability in roll motion, the moment of inertia would have to be increased by about 40 times. This is practically impossible due to constraints on the mass of the robot, which should be less than 100 g for the legs to lift it. However, in the simulation, the maximum possible water interaction force, $f_{\max}$, was used and the robot was running using the pace gait, the worst case with respect to roll. Thus, an increased moment of inertia can be a sufficient condition but not necessary. In order to determine more realistic necessary conditions, we need to carefully examine the effect of timing and the gait of the robot, and also the damping effect of the water interaction.

It was also found that the pitch motion of the robot is unstable. In order to achieve equilibrium along the pitch axis, the location of center of mass, the point where the water interactions are applied, and the ratio of the propulsion to the lift force all must be appropriately controlled. Since this robot aims to locomote on land as well as on the water, simply changing the location of the center of mass will not be sufficient to stably accomplish both tasks. Future work will be focused on achieving stability in pitch motion on both land and water.

VIII. Conclusion

A 3-D dynamic model of a bio-inspired water running robot was developed to compute the lift forces and analyze the stability of roll motion. At 50 mm separation from the water, the model generates the maximum lift force for a rigid footpad and higher lift forces for a directionally compliant footpad. When the robot can move freely in the vertical direction, the initial conditions, including separation from the water and vertical velocity, can cause the robot to submerge if the running frequency is too high. In contrast, low running frequencies cannot produce sufficient lift forces. Therefore, 7-12 Hz is found to be the range necessary to run on the water surface stably. Furthermore, due to a small moment of inertia along the roll axis, the current robot prototype is unstable. To understand the roll dynamics, a pendulum model has been used which shows that the required moment of inertia is about 1.2×10^{-3} kg m^2 for the weight of the robot and running frequencies within the stated range.

ACKNOWLEDGMENTS

The authors would like to thank to Jonghoon Park for providing *piroCORE*, simulation tools, and facilitating the analysis of the water runner motion, and the NanoRobotics Laboratory members for their support and suggestions.

References

[1] R. Suter *et al.*, "Locomotion on the water surface: Propulsive mechanisms of the fisher spider *Dolomedes Triton*," *J. of Exp. Biology*, vol. 200, pp. 2523–2538, October 1994.

[2] Y. S. Song and M. Sitti, "Surface tension driven biologically inspired water strider robots: Theory and experiments," *IEEE Tran. on Robotics and Automation*, vol. 23, pp. 578–589, June 2007.

[3] J. Bush and D. Hu, "Walking on water: Biolocomotion at the interface," *Annual Rev. of Fluid Mech*, vol. 38, pp. 339–369, January 2006.

[4] S. Floyd, T. Keegan, and M. Sitti, "A novel water running robot inspired by basilisk lizards," in *Proc. of the 2006 IEEE/RSJ Int. Conference on Intelligent Robots and Systems*, Beijing, China, November 2006, pp. 5430–5436.

[5] A. Boxerbaum, P. Werk, D. Quinn, and R. Vaidyanathan, "Design of an autonomous amphibious robot for surf zone operation," in *Proc. of the IEEE/ASME International Conference on Advanced Intelligent Mechatronics*, July 2005, pp. 1459–1464.

[6] A. Crespi, A. Badertscher, A. Guignard, and A. Ijspeert, "Amphibot 1: an amphibious snake-like robot," *Robotics and Autonomous Systems*, vol. 50, pp. 163–175, March 2005.

[7] S. Guo, T. Fukuda, and K. Asaka, "A new type of fish-like underwater microrobot," *IEEE/ASME Transactions on Mechatronics*, vol. 8, pp. 136–141, March 2003.

[8] C. Georgiadis, "Aqua: An aquatic walking robot," in *Proc. of the IEEEE/RSJ International Conference on Intelligent Robots and Systems*, September 2004, pp. 3525–3531.

[9] Y. Song, S. Suhr, and M. Sitti, "Modeling of the supporting legs for designing biomimetic water strider robots," in *Proc. of International Conference on Robotics and Automation*, May 2006, pp. 2303–2310.

[10] D. Hu, B. Chan, and J. Bush, "The hydrodynamics of water strider locomotion," *Nature*, vol. 424, pp. 663–666, August 2003.

[11] H. Takonobu, K. Kodaira, and H. Takeda, "Water striders muscle arrangement-based robot," in *IEEE/RSJ International Conference on Intelligent Robots and Systems*, August 2005, pp. 1754–1759.

[12] W. Press, S. Teukolsky, W. Vetterling, and B. Flannery, *Numerical Recipes in C++: the art of scientific computing*. Cambridge University Press, 2002.

[13] J. Park and W.-K. Chung, "Geometric integration on euclidean group with application to articulated multibody systems," *IEEE Tran. on Robotics*, vol. 21, pp. 850–863, October 2005.

[14] R. M. Murray, Z. Li, and S. S. Sastry, *A Mathematical Introduction to Robotic Manipulation*. CRC Press, Inc., 1994.

[15] J. Park, "Principle of dynamical balance for multibody systems," *Multibody System Dynamics*, vol. 14, pp. 269–299(31), November 2005.

[16] S. Floyd, S. Adilak, R. Rogman, and M. Sitti, "Performance of different foot designs for a water running robot," in *Proc. of International Conference on Robotics and Automation*, 2008.

[17] J. Glasheen and T. McMahon, "Vertical water entry of disks at low froude number," *Phys. of Fluids*, vol. 8, pp. 2078–2083, August 1996.

[18] H. Kimura, I. Shimoyama, and H. Miura, "Dynamics in the dynamic walk of a quadruped robot," *Advanced Robotics*, vol. 4, no. 3.